Alignment of a three-mirror anastigmatic telescope using nodal aberration theory

Zhiyuan Gu,[1,2,*] Changxiang Yan,[1] and Yang Wang[3]

[1]*Changchun Institute of Optics, Fine Mechanics and Physics, Chinese Academy of Science, Changchun, 130033, China*

[2]*University of Chinese Academy of Sciences, Beijing 100049, China*

[3]*School of OptoElectronic Engineering, Changchun University of Science and Technology, Changchun, 130022, China*

[*]*zhiyuan.gu@hotmail.com*

Abstract: Most computer-aided alignment methods for optical systems are based on numerical algorithms at present, which omit aberration theory. This paper presents a novel alignment algorithm for three-mirror anastigmatic (TMA) telescopes using Nodal Aberration Theory (NAT). The aberration field decenter vectors and boresight error of misaligned TMA telescopes are derived. Two alignment models based on 3rd and 5th order NAT are established successively and compared in the same alignment example. It is found that the average and the maximum RMS wavefront errors in the whole field of view of 0.3° × 0.15° are 0.063 λ (λ = 1 μm) and 0.068 λ respectively after the 4th alignment action with the 3rd order model, and 0.011 λ and 0.025 λ (nominal values) respectively after the 3rd alignment action with the 5th order model. Monte-Carlo alignment simulations are carried out with the 5th order model. It shows that the 5th order model still has good performance even when the misalignment variables are large (−1 mm≤linear misalignment≤1 mm, −0.1°≤angular misalignment≤0.1°), and multiple iterative alignments are needed when the misalignment variables increase.

OCIS codes: (110.6770) Telescopes; (220.1140) Alignment; (080.1010) Aberrations (global).

References and links

1. J. W. Figoski, T. E. Shrode, and G. F. Moore, “Computer-aided alignment of a wide-field, three-mirror, unobscured, high-resolution sensor,” Proc. SPIE **1049**, 166–177 (1989).
2. S. Kim, H.-S. Yang, Y.-W. Lee, and S.-W. Kim, “Merit function regression method for efficient alignment control of two-mirror optical systems,” Opt. Express **15**(8), 5059–5068 (2007).
3. H. Lee, G. B. Dalton, I. A. J. Tosh, and S.-W. Kim, “Computer-guided alignment II :Optical system alignment using differential wavefront sampling,” Opt. Express **15**(23), 15424–15437 (2007).
4. K. P. Thompson and J. P. Rolland, “A page from “the drawer”: how Roland Shack opened the door to the aberration theory of freeform optics,” Proc. SPIE **9186**, 91860A (2014).
5. K. P. Thompson, “Aberration fields in tilted and decentered optical systems,” Ph.D. dissertation (University of Arizona, 1980).
6. T. Schmid, K. P. Thompson, and J. P. Rolland, “Alignment induced aberration fields of next generation telescopes,” Proc. SPIE **7068**, 70680E (2008).
7. K. P. Thompson, T. Schmid, and J. P. Rolland, “The misalignment induced aberrations of TMA telescopes,” Opt. Express **16**(25), 20345–20353 (2008).
8. K. P. Thompson, T. Schmid, and J. P. Rolland, “Alignment induced aberration fields of next generation telescopes,” Proc. SPIE **6834**, 68340B (2007).
9. K. P. Thompson, K. Fuerschbach, T. Schmid, and J. P. Rolland, “Using nodal aberration theory to understand the aberrations of multiple unobscured three mirror anastigmatic (TMA) telescopes,” Proc. SPIE **7433**, 74330B (2009).
10. The Fringe Zernike polynomial was developed by John Loomis at the University of Arizona, Optical Sciences Center in the 1970s, and is described on page C-8 of the CODE V® Version 10.4 Reference Manual (Synopsys, Inc.) (2012).
11. K. P. Thompson, T. Schmid, O. Cakmakci, and J. P. Rolland, “Real-ray-based method for locating individual surface aberration field centers in imaging optical systems without rotational symmetry,” J. Opt. Soc. Am. A **26**(6), 1503–1517 (2009).

12. R. A. Buchroeder, "Tilted component optical systems," Ph.D. dissertation (University of Arizona, 1976).
13. R. K. Tyson, "Conversion of Zernike aberration coefficients to Seidel and higher-order power-series aberration coefficients," Opt. Lett. **7**(6), 262–264 (1982).
14. K. Thompson, "Description of the third-order optical aberrations of near-circular pupil optical systems without symmetry," J. Opt. Soc. Am. A **22**(7), 1389–1401 (2005).
15. K. P. Thompson, "Multinodal fifth-order optical aberrations of optical systems without rotational symmetry: spherical aberration," J. Opt. Soc. Am. A **26**(5), 1090–1100 (2009).
16. K. P. Thompson, "Multinodal fifth-order optical aberrations of optical systems without rotational symmetry: the comatic aberrations," J. Opt. Soc. Am. A **27**(6), 1490–1504 (2010).
17. K. P. Thompson, "Multinodal fifth-order optical aberrations of optical systems without rotational symmetry: the astigmatic aberrations," J. Opt. Soc. Am. A **28**(5), 821–836 (2011).
18. J. Sasián, "Theory of sixth-order wave aberrations," Appl. Opt. **49**(16), D69–D95 (2010).

1. Introduction

With the development of astronomy, the need for the high resolution, depth and breadth of astronomical observations grow rapidly. People take the more and more high request to the image quality and field of view of space telescope. Reflecting systems are commonly used in the design of large aperture space telescopes (e.g. Hubble telescope and James Webb Space Telescope (JWST)) because they are completely free of chromatic aberration.

More than 100 years ago, large two-mirror telescopes first appeared. Up to now, most large astronomical telescopes for professional use are two-mirror forms with either a parabolic (Cassegrain) or a hyperbolic (Ritchey-Chretien) primary mirror. For Cassegrain telescopes, the field of view is limited by coma aberration with a linear field dependence, and for the Ritchey-Chretien telescopes, the field of view is limited by uncorrected third-order astigmatism which increases quadratically with field of view. So two-mirror systems cannot meet the requirements of wide field and near diffraction-limit imaging quality. Compared with two-mirror systems, the TMA telescopes are corrected for four aberrations: spherical aberration, coma, astigmatism, and field curvature, so they have a wider field of view. They have occupied an important position in the design of space telescope in recent years. In general, TMA telescopes come in two forms: field bias and aperture offset. The next major space-borne observatory, the JWST, is a representative field-biased TMA telescope.

A good alignment state is the precondition of the telescope with excellent observation performance. Compared with two-mirror systems, TMA systems have more alignment degrees of freedom which are more difficult to align. For space-based telescopes, the accurate alignment algorithm is the assurance of good performance of telescopes whether in the prelaunch alignment or the on-orbit alignment. It is urgent to provide an alignment algorithm for this class of telescopes. In this paper, our aim is to develop an alignment algorithm for the field-biased TMA telescopes which are similar to the JWST.

At present, there are many alignment theories for imaging system. Figoski et al. [1] used sensitivity table method for alignment of a wide field, three-mirror system. The alignment optimization in commercial optical design software Code V also works with this method. Seonghui Kim et al. [2] pointed out the sensitivity table method can't bring high accuracy to the estimation of the misalignment parameters if the misalignment values are large, as a result of the nonlinearity of the Zernike coefficient sensitivity to the alignment parameters. Then he presented a new merit function regression method, which utilizes the merit function consisting of Zernike coefficients representing the misaligned optical wavefronts, and attempts to minimize merit function using actively damped least square algorithm to estimate the misalignment states. Furthermore, Hanshin Lee et al. [3] introduced differential wavefront sampling method for the efficient alignment of centred optical systems. All the methods above are based on data reduction and numerical methods but without a tie to aberration theory.

NAT is a powerful tool to study optical systems that contain misaligned, or intentionally tilted and/or decentered components. In 1976, Shack discovered binodal astigmatism in through-focus star plate taken with the 90" Bok telescope on Kitt Peak [4]. In 1980, Thompson [5] described the wavefront aberrations (expanded up to 5th order) that can occur in non-symmetric optical systems. Schmid et al. [6] demonstrated how nodal aberration

#244275 Received 23 Jul 2015; revised 2 Sep 2015; accepted 2 Sep 2015; published 17 Sep 2015

theory can be used to determine the aberration field dependencies for misaligned TMA telescopes. Their results show that two dominant 3rd order misalignment aberrations arise for any TMA telescope, field-constant coma and field-linear, field-asymmetric astigmatism. They also pointed out that the alignment of TMA telescopes cannot be accomplished using on-axis performance data alone. Similar conclusions can be found in [7]. Another important conclusion shown in [6] is that if a TMA telescope is aligned to remove axial coma and under this condition if astigmatism is measured on-axis this astigmatism is due to astigmatic mirror figure error and is not due to misalignment. Thompson et al. [8] proposed an alignment strategy based on aberration compensation for TMA telescopes. The application of NAT to understanding the optical design of an optical system with a chain of four TMA telescopes is discussed in [9]. These analysis and conclusions provide theoretic guidance for alignment of TMA systems. However, the quantitative calculation for misalignments has not been discussed in the previous researches.

In this paper, we take a TMA telescope as an example and use NAT to study the calculation for misalignments. Section 2 describes the optical parameters of the TMA telescope. Section 3 derives aberration field decenter vectors and boresight error for a misaligned TMA system based on NAT. In Section 4, we establish the alignment model based on 3rd order NAT, and analyze its shortcomings by an alignment example. In Section 5, we propose another alignment model based on 5th order NAT, and give a comparison of it to the 3rd order model. In section 6, we discuss the alignment capability of the 5th order model in different ranges of misalignments by Monte-Carlo simulations. We summarize our findings in Section 7. The Appendix supplies a compilation of the acronyms and mathematical symbols that are used throughout the paper.

2. Optical parameters for the TMA telescope

The TMA telescope (see Fig. 1) used for alignment simulation in our paper is similar to JWST. It is a 6.6 meter F/14 TMA telescope with a 0.3° × 0.15° field of view and a 0.18° field offset. The aperture stop located on the primary mirror (PM). The PM, the secondary mirror (SM) and the tertiary mirror (TM) have a common axis of rotational symmetry, which is slightly different from the JWST which has a decentered TM and a curved image surface. Table 1 shows the optical prescription of the example system. A right-handed coordinate system is defined in Fig. 1. The optical axis of the telescope (the common axis of rotational symmetry of the PM, the SM and the TM) is z-axis, and the light starts out from the object travels in the + z direction.

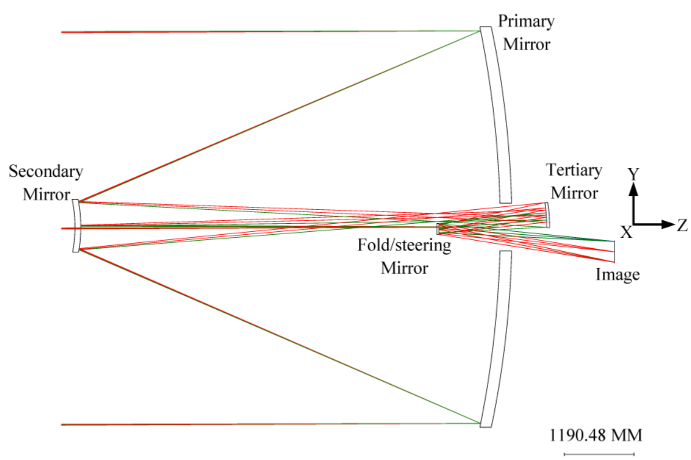

Fig. 1. The optical layout of the TMA telescope.

#244275 Received 23 Jul 2015; revised 2 Sep 2015; accepted 2 Sep 2015; published 17 Sep 2015

Table 1. Optical Prescription of the Example System

Surface	Type	Conic constant	Radius (mm)	Thickness (mm)
PM (stop)	Conic	−0.9948	−16287.099	−7170
SM	Conic	−1.8351	−2317.426	7965
TM	Conic	−0.7202	−2702.327	−1845
fold/steering mirror			Flat	3006.205
image			Flat	

The fold/steering mirror is decentered 32.759 mm from the optical axis, towards the focal surface center.

The nominal performance of the TMA over the field is shown in Figs. 2(a)-2(c). Fringe Zernike coefficients [10] $C_{5/6}$ (related to astigmatism), $C_{7/8}$ (related to coma) and RMS wavefront error are characterized and visualized through Full-Field-Displays (FFDs) in Figs. 2(a)-2(c), respectively. For the telescope, note that only the portion of the field in the red dashed boxes is utilized, but a larger portion of the field is shown for the better understanding of the aberration fields. In Figs. 2(a) and 2(b), we can find coma and astigmatism is zero at the field center and at a ring-shaped zone in the field, where third, fifth and higher order aberrations balance each other.

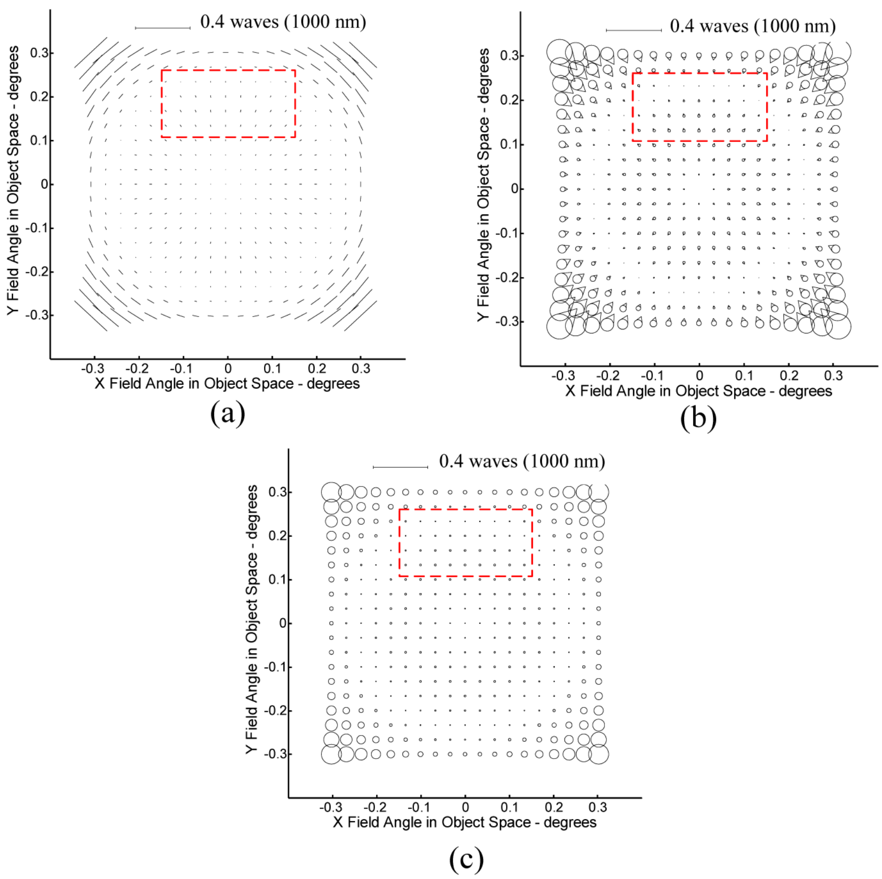

Fig. 2. FFDs for Fringe Zernike coefficients (a) $C_{5/6}$, (b) $C_{7/8}$, and (c) RMS wavefront error for the nominal TMA telescope.

In our paper, we can choose the TM as a reference without loss of generality, and assume it is fixed. The PM and the SM are misaligned relative to the TM. Because the TMA is a symmetrical optical system about z-axis, the rotation of optical elements about z-axis (*CDE*) will not affect its optical properties, so this type of misalignments is invalid. The decenter of optical elements along z-axis (*ZDE*) only cause rotationally symmetric aberrations (such as defocus or spherical aberration). This type of misalignments can be solved with the aberration theory for symmetrical optical system. This paper will not discuss them. We only focus on the misalignments that can break the axial symmetry of the optical system. This type of misalignments in telescope are the decenter of PM and SM along x-axis and y-axis (*XDE* and *YDE*), the tilts of PM and SM in y-z plane and x-z plane (*ADE* and *BDE*), respectively. Note that a positive *XDE/YDE* is the displacement in the + x/y direction, and a positive *ADE/BDE* is the rotation which is left-handed about the + x/y axis.

3. Aberration field decenter vectors and boresight error

It is well known that in the theory of 3rd order aberrations of rotationally symmetric optical systems the total aberrations can be described as the summation over all individual surface-by-surface contributions. The field dependence of all of the 3rd order aberrations of an individual spherical optical surface is rotationally symmetric about a common axis for each surface. The common axis is called as the optical axis of the system.

According to NAT, when an imaging optical system with a circular pupil is perturbed, no new aberrations will be created, but the centers of the aberration field contribution for each surface in the system no longer coincide, and the behavior of the aberration field at the image plane will be modified.

The vector form of wave aberration expansion in misaligned optical systems are expressed by [5,11]

$$W=\sum_{j}\sum_{p}^{\infty}\sum_{n}^{\infty}\sum_{m}^{\infty}W_{klm,j}^{(sph,asph)}\left(\vec{H}_{Aj}^{(sph,asph)}\cdot\vec{H}_{Aj}^{(sph,asph)}\right)^{p}\left(\vec{\rho}\cdot\vec{\rho}\right)^{n}\left(\vec{H}_{Aj}^{(sph,asph)}\cdot\vec{\rho}\right)^{m},\quad k=2p+m, l=2n+m, \tag{1}$$

where the subscript j is the surface number, $W_{klm,j}$ is the wave aberration coefficient for surface j, $\vec{H}_{Aj}$ denotes the effective field height for surface j, and $\vec{\rho}$ is the normalized vector describing the position in the pupil. $\vec{H}_{Aj}$ and $\vec{\rho}$ are visualized in Fig. 3. Note that a fundamental concept in NAT is the decomposition of the surface wave aberration contributions into two separate contributions each, one associated with the spherical base curve, the other determined by the aspheric departure (if any) from the spherical base curve. The superscript *sph* and *asph* are used to distinguish them.

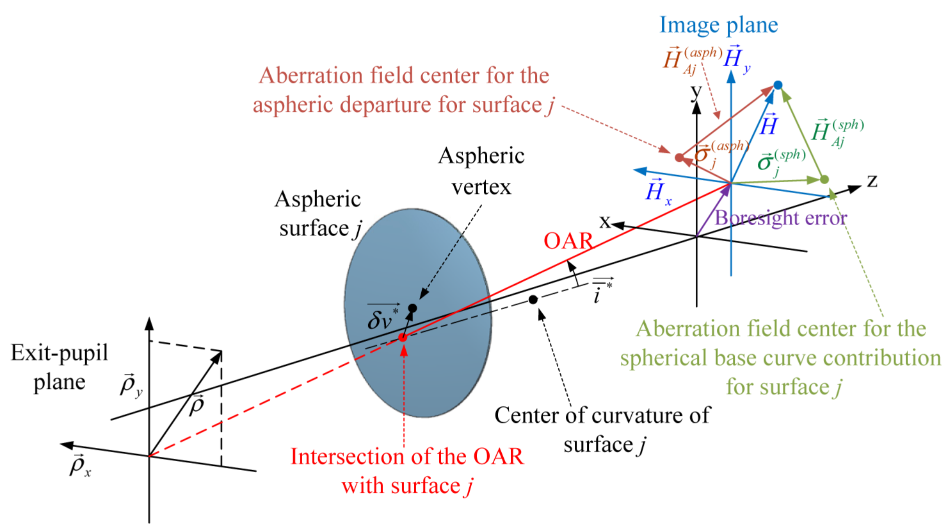

Fig. 3. Concepts of effective field height, aberration field decenter vectors and boresight error.

#244275 Received 23 Jul 2015; revised 2 Sep 2015; accepted 2 Sep 2015; published 17 Sep 2015

In a misaligned or generally nonsymmetric optical system made of otherwise rotationally symmetric optical surfaces, the optical axis ray (OAR) is defined as the ray that connects the center of the object with the center of the circular physical aperture stop within the optical system, which is typically called as chief ray for the on-axis field point.

In Eq. (1), the effective field height vector $\vec{H}_{Aj}^{(sph,asph)}$ is given by

$$\vec{H}_{Aj}^{(sph,asph)} = \vec{H} - \vec{\sigma}_j^{(sph,asph)}. \tag{2}$$

The vector $\vec{\sigma}_j^{(sph,asph)}$ was first introduced by Buchroeder [4,12], which represents the decentration of the center of the aberration field of surface with respect to the OAR intercept with the Gaussian image plane, as visualized in Fig. 3. It depends on the misalignments of optical elements, which is called aberration field decenter vector.

For the spherical surface contribution to the aberration field, as detailed by Thompson [5,11], the location of the center of symmetry for the surface contribution is given by

$$\vec{\sigma}_j^{(sph)} = -\frac{\overrightarrow{\bar{i}_j^*}}{\bar{i}_j} = -\frac{\overrightarrow{\bar{u}_{OAR\ j}^{\#}} - \overrightarrow{\beta_{0\ j}^{\#}} + \overrightarrow{\bar{y}_{OAR\ j}^{\#}} \cdot c_j}{\bar{u}_j + \bar{y}_j c_j}, \tag{3}$$

where $\overrightarrow{\bar{i}_j^*}$ denotes the incident angle of the OAR at surface j, $\bar{i}_j$ denotes the paraxial incident angle of the chief ray at surface j, $\overrightarrow{\bar{u}_{OAR\ j}^{\#}}$ denotes the OAR paraxial angle prior to surface j referenced to the z-axis. $\overrightarrow{\bar{y}_{OAR\ j}^{\#}}$ denotes the OAR intersection height at surface j referenced to the z-axis, c_j denotes the curvature of surface j. $\bar{u}_j$ corresponds to paraxial chief ray angle incident at surface j, $\bar{y}_j$ corresponds to the paraxial chief ray height at surface j, and $\overrightarrow{\beta_{0\ j}^{\#}}$ corresponds to the equivalent tilt of surface j [11], is given by

$$\overrightarrow{\beta_{0\ j}^{\#}} = \begin{bmatrix} -BDE_j + XDE_j c_j \\ ADE_j + YDE_j c_j \end{bmatrix}. \tag{4}$$

The paraxial quantities $\bar{u}_j$ and $\bar{y}_j$ can be derived by utilizing traditional paraxial equations for rotationally symmetric optical systems, which are given by

$$\bar{u}_{SM} = -\bar{u}_{PM}, \tag{5}$$

$$\bar{u}_{TM} = \frac{\bar{u}_{PM}\left(2d_1 + r_{SM}\right)}{r_{SM}}, \tag{6}$$

$$\bar{y}_{PM} = 0, \tag{7}$$

$$\bar{y}_{SM} = -d_1 \bar{u}_{PM}, \tag{8}$$

$$\bar{y}_{TM} = \frac{2d_1 d_2 \bar{u}_{PM}}{r_{SM}} - \bar{u}_{PM}\left(d_1 - d_2\right), \tag{9}$$

where r_j denotes the radius of surface j, d_j denotes the thickness of surface j.

The location of the aspheric contribution is located at

$$\vec{\sigma}_j^{(asph)} = \frac{\overrightarrow{\delta v_j^*}}{\bar{y}_j} = \frac{1}{\bar{y}_j}\left(\begin{bmatrix} XDE_j \\ YDE_j \end{bmatrix} - \overrightarrow{\bar{y}_{OAR\ j}^{\#}}\right), \tag{10}$$

where $\overrightarrow{\delta v_j^*}$ denotes the intersection height of the OAR with respect to the aspheric vertex of surface j.

The OAR quantities $\overrightarrow{\bar{u}^{\#}_{OAR\ j}}$ and $\overrightarrow{\bar{y}^{\#}_{OAR\ j}}$ can be computed using the LCS paraxial ray-trace equations for optical systems with tilted and decentered surfaces as developed by Buchroeder [11,12] or a real ray computed using Snell's law as in any commercial optical design software package. In this paper, paraxial ray-trace method is used to obtain the analytical expressions for aberration field decenter vectors and boresight error. $\overrightarrow{\bar{u}^{\#}_{OAR\ j}}$ and $\overrightarrow{\bar{y}^{\#}_{OAR\ j}}$ are given by

$$\overrightarrow{\bar{u}^{\#}_{OAR\ PM}} = \begin{bmatrix} 0 \\ 0 \end{bmatrix}, \tag{11}$$

$$\overrightarrow{\bar{u}^{\#}_{OAR\ SM}} = \begin{bmatrix} -2\,BDE_{PM} \\ 2\,ADE_{PM} \end{bmatrix}, \tag{12}$$

$$\overrightarrow{\bar{u}^{\#}_{OAR\ TM}} = \begin{bmatrix} -2\,BDE_{SM} \\ 2\,ADE_{SM} \end{bmatrix} - \frac{2}{r_{SM}} \begin{bmatrix} XDE_{PM} \\ YDE_{PM} \end{bmatrix} + \frac{2}{r_{SM}} \begin{bmatrix} XDE_{SM} \\ YDE_{SM} \end{bmatrix} + \left(\frac{4\,d_1}{r_{SM}} + 2 \right) \begin{bmatrix} BDE_{PM} \\ -ADE_{PM} \end{bmatrix}, \tag{13}$$

$$\overrightarrow{\bar{y}^{\#}_{OAR\ PM}} = \begin{bmatrix} XDE_{PM} \\ YDE_{PM} \end{bmatrix}, \tag{14}$$

$$\overrightarrow{\bar{y}^{\#}_{OAR\ SM}} = \begin{bmatrix} XDE_{PM} - 2\,BDE_{PM}\,d_1 \\ YDE_{PM} + 2\,ADE_{PM}\,d_1 \end{bmatrix}, \tag{15}$$

$$\begin{aligned} \overrightarrow{\bar{y}^{\#}_{OAR\ TM}} = {} & d_2 \begin{bmatrix} -2\,BDE_{SM} \\ 2\,ADE_{SM} \end{bmatrix} + \left(2\,d_2 - 2\,d_1 + \frac{4\,d_1\,d_2}{r_{SM}} \right) \begin{bmatrix} BDE_{PM} \\ -ADE_{PM} \end{bmatrix}. \\ & - \left(\frac{2\,d_2}{r_{SM}} - 1 \right) \begin{bmatrix} XDE_{PM} \\ YDE_{PM} \end{bmatrix} + \frac{2\,d_2}{r_{SM}} \begin{bmatrix} XDE_{SM} \\ YDE_{SM} \end{bmatrix} \end{aligned} \tag{16}$$

The aberration field decenter vectors for PM, SM and TM can be obtained after substituting Eq. (4), the expressions for the OAR quantities (Eqs. (11)-(16)) and the paraxial quantities (Eqs. (5)-(9)) into Eqs. (3) and (10), which are given by

$$\vec{\sigma}^{sph}_{PM} = \frac{1}{\bar{u}_{PM}} \begin{bmatrix} -BDE_{PM} \\ ADE_{PM} \end{bmatrix}, \tag{17}$$

$$\vec{\sigma}^{sph}_{SM} = \frac{1}{\bar{u}_{PM}} \begin{bmatrix} -2BDE_{PM} \\ 2ADE_{PM} \end{bmatrix} + \frac{1}{\bar{u}_{PM}\left(d_1 + r_{SM}\right)} \begin{bmatrix} XDE_{PM} - XDE_{SM} + BDE_{SM}\,r_{SM} \\ -YDE_{SM} + YDE_{PM} - ADE_{SM}\,r_{SM} \end{bmatrix}, \tag{18}$$

$$\vec{\sigma}^{sph}_{TM} = \frac{1}{\bar{u}_{PM}} \begin{bmatrix} -2BDE_{PM} \\ 2ADE_{PM} \end{bmatrix} + \frac{\begin{bmatrix} BDE_{SM}\left(2d_2 r_{SM} + 2r_{SM} r_{TM}\right) + XDE_{PM}\left(2d_2 - r_{SM} + 2r_{TM}\right) - XDE_{SM}\left(2d_2 + 2r_{TM}\right) \\ -ADE_{SM}\left(2d_2 r_{SM} + 2r_{SM} r_{TM}\right) + YDE_{PM}\left(2d_2 - r_{SM} + 2r_{TM}\right) - YDE_{SM}\left(2d_2 + 2r_{TM}\right) \end{bmatrix}}{\bar{u}_{PM}\left(2d_1 d_2 - d_1 r_{SM} + d_2 r_{SM} + 2d_1 r_{TM} + r_{SM} r_{TM}\right)}, \tag{19}$$

$$\vec{\sigma}^{asph}_{PM} = \begin{bmatrix} 0 \\ 0 \end{bmatrix}, \tag{20}$$

$$\vec{\sigma}^{asph}_{SM} = \frac{1}{d_1 \bar{u}_{PM}} \begin{bmatrix} XDE_{PM} - XDE_{SM} - 2BDE_{PM}\,d_1 \\ YDE_{PM} - YDE_{SM} + 2ADE_{PM}\,d_1 \end{bmatrix}, \tag{21}$$

#244275 Received 23 Jul 2015; revised 2 Sep 2015; accepted 2 Sep 2015; published 17 Sep 2015

$$\vec{\sigma}_{TM}^{asph} = \frac{1}{\bar{u}_{PM}}\begin{bmatrix} -2BDE_{PM} \\ 2ADE_{PM} \end{bmatrix} + \frac{\begin{bmatrix} -2\,XDE_{SM}\,d_2 + XDE_{PM}\left(2d_2 - r_{SM}\right) + 2\,BDE_{SM}\,d_2\,r_{SM} \\ -2\,YDE_{SM}\,d_2 + YDE_{PM}\left(2d_2 - r_{SM}\right) - 2\,ADE_{SM}\,d_2\,r_{SM} \end{bmatrix}}{\bar{u}_{PM}\left(2\,d_1\,d_2 - d_1\,r_{SM} + d_2\,r_{SM}\right)}. \tag{22}$$

If the TMA is misaligned, not only will the behavior of the aberration field be modified, but also the image plane displacement (boresight error) will appear, as shown in Fig. 3. The intersection of the OAR with the image plane determines the boresight error relative to the z axis. It can also be derived by paraxial ray tracing of OAR, which is given by

$$\begin{aligned} \Delta\vec{H}_{IMG} = & \left(\frac{\left(4d_2 d_3 - 4d_1 d_3 + 2d_1 r_{TM} - 2d_2 r_{TM} + 2d_3 r_{TM}\right)}{r_{TM}} + \frac{4d_1\left(2d_2 d_3 - d_2 r_{TM} + d_3 r_{TM}\right)}{r_{SM}\, r_{TM}}\right)\begin{bmatrix} -BDE_{PM} \\ ADE_{PM} \end{bmatrix} \\ & -\left(\frac{\left(2d_3 - r_{TM}\right)}{r_{TM}} - \frac{\left(4d_2 d_3 - 2d_2 r_{TM} + 2d_3 r_{TM}\right)}{r_{SM}\, r_{TM}}\right)\begin{bmatrix} XDE_{PM} \\ YDE_{PM} \end{bmatrix} \\ & + \frac{\left(4d_2 d_3 - 2d_2 r_{TM} + 2d_3 r_{TM}\right)}{r_{TM}}\begin{bmatrix} BDE_{SM} \\ -ADE_{SM} \end{bmatrix} - \frac{\left(4d_2 d_3 - 2d_2 r_{TM} + 2d_3 r_{TM}\right)}{r_{SM} r_{TM}}\begin{bmatrix} XDE_{SM} \\ YDE_{SM} \end{bmatrix} \end{aligned} \tag{23}$$

4. Alignment model based on 3rd order NAT

4.1 Coma

There are two 3rd order aberrations in a misaligned TMA telescope. One is the 3rd order coma (W_{131}), which is constant in magnitude and orientation over the field. The other is the 3rd order astigmatism (W_{222}), which is field-asymmetric in orientation and increases linearly with field [6,7]. The coma is given by

$$W_{COMA_3} = [(W_{131}\vec{H} - \vec{A}_{131})\cdot\vec{\rho}](\vec{\rho}\cdot\vec{\rho}), \tag{24}$$

where $W_{131} = \sum_j W_{131j}$, $\vec{A}_{131} = \sum_j W_{131j}\vec{\sigma}_j$.

In optical testing, the wavefront at exit pupil is usually fitted to a Zernike polynomial as a representation of the measured wavefront. So Eq. (24) should be rewritten as a new form that contains the Zernike coefficients. Note that the exact correspondence between the Seidel coefficients and Zernike polynomials is generally an infinite sum [13]. But in the TMA system, the high order Zernike coefficients that are fitted against the wavefront are reasonably small, so they can be ignored. In our paper, only the first 16 items of Fringe Zernike coefficients are considered.

According to vector multiplication [14] of NAT, Eq. (24) can be rewritten as

$$W_{COMA_3} = \begin{bmatrix} W_{131}\vec{H}_x - \vec{A}_{131,x} \\ W_{131}\vec{H}_y - \vec{A}_{131,y} \end{bmatrix}\cdot\begin{bmatrix} |\vec{\rho}|^3\cos\varphi \\ |\vec{\rho}|^3\sin\varphi \end{bmatrix}, \tag{25}$$

where $\vec{A}_{131,x}$ and $\vec{A}_{131,y}$ are the x-component and the y-component of $\vec{A}_{131}$, respectively. According to the relationship between Seidel coefficients and Zernike coefficients, we can find that

$$\begin{bmatrix} \vec{A}_{131,x} \\ \vec{A}_{131,y} \end{bmatrix} = \begin{bmatrix} W_{131}\vec{H}_x - 3C_{COMA,x} \\ W_{131}\vec{H}_y - 3C_{COMA,y} \end{bmatrix}, \tag{26}$$

where $\begin{bmatrix} C_{COMA,x} \\ C_{COMA,y} \end{bmatrix} = \begin{bmatrix} C_7 - C_{10} - 4C_{14} \\ C_8 - C_{11} - 4C_{15} \end{bmatrix}$, and C_i is the i^{th} Fringe Zernike coefficient.

#244275 Received 23 Jul 2015; revised 2 Sep 2015; accepted 2 Sep 2015; published 17 Sep 2015

W_{131} can be calculated by Seidel formula, which is given in Table 2. Only $\vec{A}_{131,x}$ and $\vec{A}_{131,y}$ need to be solved. For each wavefront measurement, two equations can be obtained, so one wavefront measurement is sufficient to fully characterize the coma aberration field.

Table 2. Third Order Aberration Coefficients of the TMA Telescope

	$W_{131,j}^{sph}$	$W_{131,j}^{asph}$	$W_{222,j}^{sph}$	$W_{222,j}^{asph}$
PM(stop)	−447.721	0	6.768	0
SM	214.671	218.448	−14.395	15.357
TM	4.036	10.745	14.326	−21.921
sum	0.179		0.135	

The aberration coefficients are computed at a field angle of 0.18°, at a wavelength of 1 μm, which are in waves.

4.2 Astigmatism

Similar to 3rd order coma, the astigmatism is given by

$$W_{AST_3}=\frac{1}{2}[\sum_j W_{222j}\vec{H}^2-2\vec{H}A_{222}+\vec{B}_{222}^2]\cdot\vec{\rho}^2, \tag{27}$$

where $W_{222}=\sum_j W_{222j}$, $\vec{A}_{222}=\sum_j W_{222j}\vec{\sigma}_j$, $\vec{B}_{222}^2=\sum_j W_{222j}\vec{\sigma}_j^{\,2}$.

According to vector multiplication of NAT, Eq. (27) can be rewritten as

$$W_{AST_3}=\begin{bmatrix}\dfrac{W_{222}\left(\vec{H}_x^2-\vec{H}_y^2\right)}{2}-\vec{H}_x\vec{A}_{222,x}+\vec{H}_y\vec{A}_{222,y}+\dfrac{\vec{B}_{222,x}^2}{2}\\ W_{222}\vec{H}_x\vec{H}_y-\vec{H}_x\vec{A}_{222,y}-\vec{H}_y\vec{A}_{222,x}+\dfrac{\vec{B}_{222,y}^2}{2}\end{bmatrix}\cdot\begin{bmatrix}|\vec{\rho}|^2\cos(2\varphi)\\ |\vec{\rho}|^2\sin(2\varphi)\end{bmatrix}. \tag{28}$$

According to the relationship between Seidel coefficients and Zernike coefficients, we may find that

$$\begin{bmatrix}-\vec{H}_x & \vec{H}_y & \dfrac{1}{2} & 0\\ -\vec{H}_y & -\vec{H}_x & 0 & \dfrac{1}{2}\end{bmatrix}\begin{bmatrix}\vec{A}_{222,x}\\ \vec{A}_{222,y}\\ \vec{B}_{222,x}^2\\ \vec{B}_{222,y}^2\end{bmatrix}=\begin{bmatrix}C_{AST,x}-\dfrac{W_{222}}{2}\left(\vec{H}_x^2-\vec{H}_y^2\right)\\ C_{AST,\mathrm{y}}-W_{222}\vec{H}_x\vec{H}_y\end{bmatrix}, \tag{29}$$

where $\begin{bmatrix}C_{AST,x}\\ C_{AST,\mathrm{y}}\end{bmatrix}=\begin{bmatrix}C_5-3C_{12}\\ C_6-3C_{13}\end{bmatrix}$.

W_{222} is given in Table 2. Consequently, there are 4 unknowns: $\vec{A}_{222,x}$, $\vec{A}_{222,y}$, $\vec{B}_{222,x}^2$ and $\vec{B}_{222,y}^2$. In order to fully characterize the astigmatic aberration field, wavefront measurements at a minimum of two field points are required.

Utilizing Eqs. (17)-(23), (26) and (29), if the wavefronts are measured at multiple field points, an overdetermined system of nonlinear equations with 8 unknown misalignments can be established. In our paper, the medium-scale fminunc algorithm in the MATLAB Optimization Toolbox is used to solve the system of nonlinear equations.

4.3 Alignment example

In this section, we introduce a set of misalignments randomly, and conduct an alignment simulation of the TMA telescope. The misalignments are given in Table 3.

#244275 Received 23 Jul 2015; revised 2 Sep 2015; accepted 2 Sep 2015; published 17 Sep 2015

Table 3. Misalignments of the TMA Telescope

XDE_{PM}	YDE_{PM}	ADE_{PM}	BDE_{PM}	XDE_{SM}	YDE_{SM}	ADE_{SM}	BDE_{SM}
0.03	−0.04	−0.011	0.009	0.025	0.3	−0.04	0.075

XDE and *YDE* are in mm while *ADE* and *BDE* are in degree.

Each of these misalignments is introduced in the software Code V and the wavefront and boresight error can be obtained. To each wavefront a Fringe Zernike polynomial of 37 terms are adjusted. In the misaligned state, $C_{5/6}$ and $C_{7/8}$ of the TMA are characterized and visualized through the use of FFDs in Figs. 4(a) and 4(b).

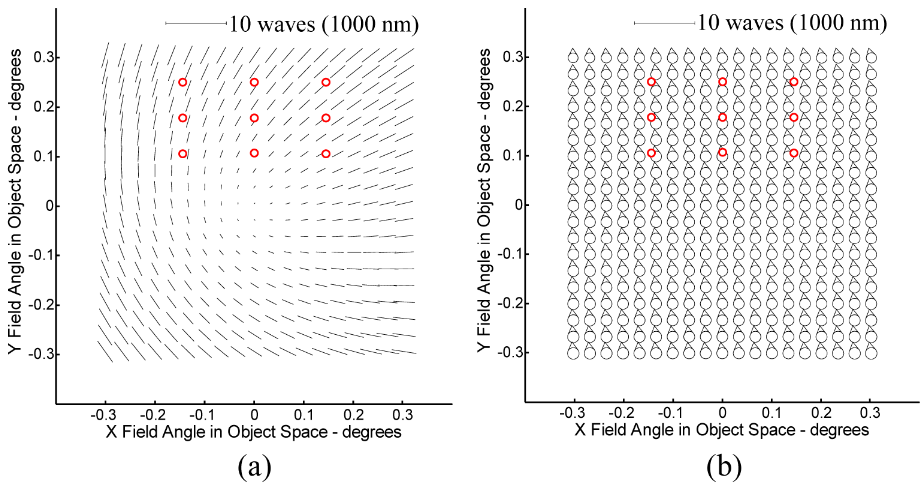

Fig. 4. FFDs for Fringe Zernike coefficients (a) $C_{5/6}$ and (b) $C_{7/8}$ for the misaligned TMA telescope.

Now we use the 3rd order model to solve the misalignments. In the simulation calculation, 9 measured field points are used, which are circled in red in Figs. 4(a) and 4(b). The 3rd order aberration coefficients used in the alignment corrections are given in Table 2. We make 5 alignments on the misaligned TMA in a row. The absolute values of residual misalignments of TMA after each alignment action are shown in the Figs. 5(a) and 5(b). The change of RMS wavefront error is shown in Fig. 5(c). Note that 361(19 × 19) equally spaced field points in 0.3° × 0.15° are used to calculate the average and maximum RMS wavefront error.

#244275 Received 23 Jul 2015; revised 2 Sep 2015; accepted 2 Sep 2015; published 17 Sep 2015

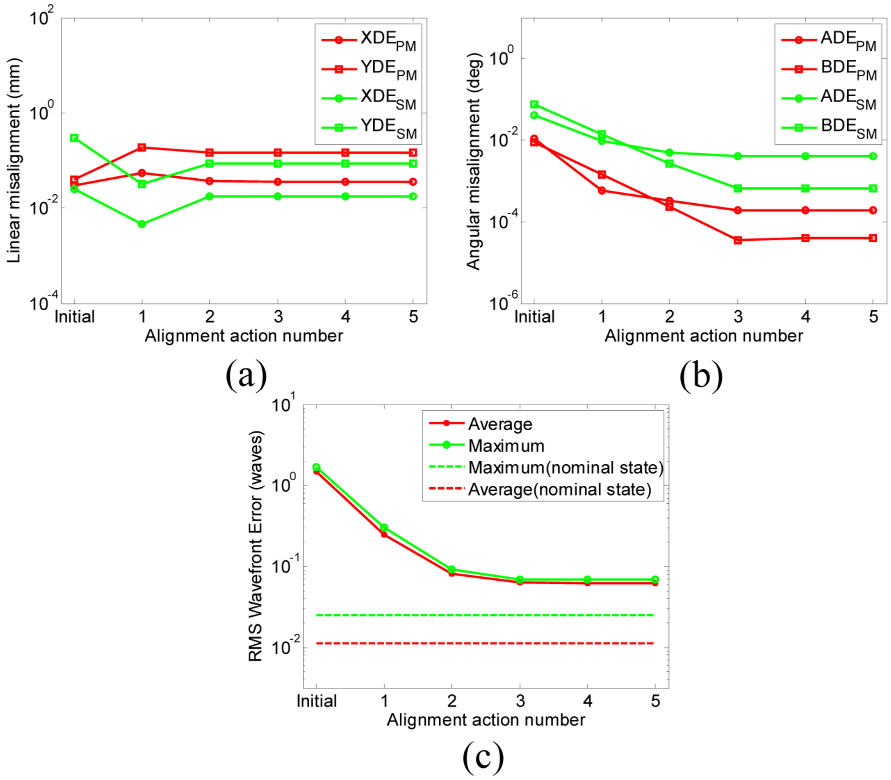

Fig. 5. The results after each alignment action. (a) The residual linear misalignments (b) The residual angular misalignments (c) The residual RMS wavefront error.

It can be seen from Fig. 5 (a) that the residual linear misalignments exhibit alternating behaviors in the first two alignment actions and reach steady states basically after the 2nd alignment action. The Figs. 5(b) and 5(c) show that the residual angular misalignments and the wavefront error show declining trends in the first three alignment actions and reach steady states after the 3rd alignment action. After the 4th alignment action, the residual errors of ADE_{PM}, BDE_{PM}, ADE_{SM} and BDE_{SM} are –0.0002°, –0.0001°, –0.0041° and 0.0007°, respectively; and the residual errors of XDE_{PM}, YDE_{PM}, XDE_{SM} and YDE_{SM} are 0.0019 mm, 0.1459 mm, –0.0116 mm and 0.0861 mm. It can be found that the calculation of angular misalignments is more accurate than the linear ones, and the calculation of angular misalignments of PM is more accurate than that of SM. In the whole field of view of 0.3° × 0.15°, the average and maximum RMS wavefront error of the nominal system are 0.011 λ and 0.025 λ (λ = 1 μm, similarly hereinafter). As seen in Fig. 5(c), after the 4th alignment action, the residual RMS wavefront error reaches the minimum: the average RMS wavefront error is 0.063 λ, and the maximum RMS wavefront error is 0.068 λ. Compared with the nominal state, a great gap still exists. So the alignment is unsuccessful.

After the 4th alignment action, $C_{5/6}$ and $C_{7/8}$ of the TMA are visualized through the use of FFDs in Figs. 6(a) and 6(b). Compared with the misaligned state before alignment corrections (Figs. 4(a) and 4(b)), it can be seen that, two dominant misalignment aberrations arise for the original misaligned TMA telescope, which are field-constant 3rd order coma and field-asymmetric, field-linear, 3rd order astigmatism. The results are in accord with the conclusions in [6,7]. After the 4th alignment action, the 3rd order misalignment aberrations decrease a lot. The magnitude of astigmatism still has an approximate linear relationship with the field of view, but in the coma aberration field neither the magnitude nor the orientation is constant. The coma is small at a ring-shaped zone in the field. This is because the effects of higher order aberrations begin to emerge. The 3rd order NAT cannot characterize the coma aberration field which is shown in Fig. 6(b) accurately. If the 3rd order model continues to be used for alignment, the wavefront error can't converge any further. So the higher order aberrations (e.g. 5th order aberration) should be introduced in the alignment model.

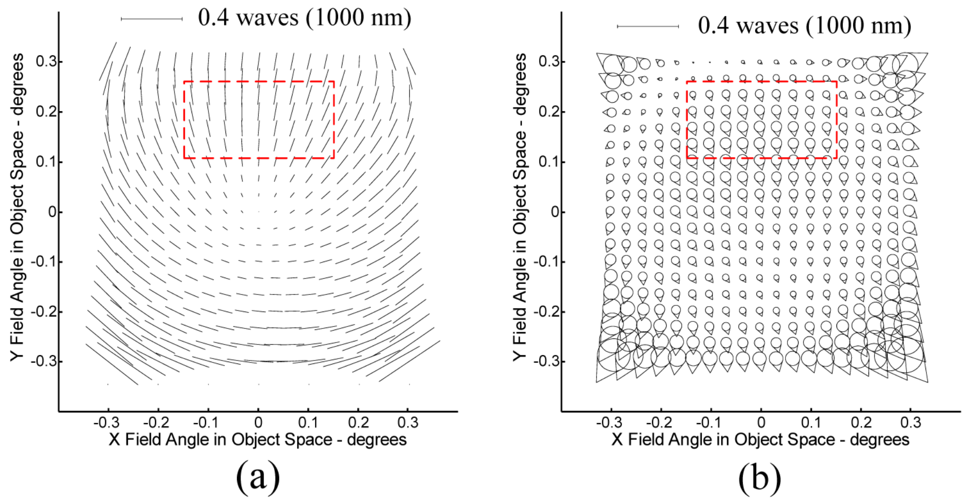

Fig. 6. FFDs for Fringe Zernike coefficients (a) $C_{5/6}$ and (b) $C_{7/8}$ for the TMA telescope after the 4th alignment action.

From the analyses made above, we can conclude that the 3rd order model is effective when the field-constant 3rd order coma and the field-linear 3rd order astigmatism are dominant misalignment aberrations in the early phase of alignment correction. After the 3rd alignment action, most of the misalignment aberrations are corrected, and higher order aberrations should be considered to get better performance. In the next section, 5th order aberrations will be added in the alignment model.

5. Alignment model based on 5th order NAT

5.1 Coma

The 5th order NAT has more complex forms compared with the 3rd order. Thompson [15–17] analyzed the nodal aberration characteristics of 5th order optical aberration fields of the misaligned optical system in detail. In the 5th order wave aberration expansions, the item which has the same aperture dependence as 3rd order coma is field-cubed coma (W_{331M}). Its wave aberration expansion is

$$W_{COMA_5}=\begin{bmatrix} W_{331M}\left(\vec{H}\cdot\vec{H}\right)\vec{H}-2\left(\vec{H}\cdot\vec{A}_{331M}\right)\vec{H}+2B_{331M}\vec{H} \\ -\left(\vec{H}\cdot\vec{H}\right)\vec{A}_{331M}+\vec{B}^{2}_{331M}\vec{H}^{*}-\vec{C}_{331M} \end{bmatrix}\cdot\vec{\rho}\left(\vec{\rho}\cdot\vec{\rho}\right), \qquad (30)$$

where $W_{331M}=\sum_j W_{331Mj}$, $\vec{A}_{331M}=\sum_j W_{331Mj}\vec{\sigma}_j$, $B_{331M}=\sum_j W_{331Mj}\left(\vec{\sigma}_j\cdot\vec{\sigma}_j\right)$, $\vec{B}^{2}_{331M}=\sum_j W_{331Mj}\vec{\sigma}_j^{\,2}$, $\vec{C}_{331M}=\sum_j W_{331Mj}\left(\vec{\sigma}_j\cdot\vec{\sigma}_j\right)\vec{\sigma}_j$, $\vec{H}^{*}$ is complex conjugate of $\vec{H}$.

We can sum the 3rd order coma and the field-cubed coma together, and merge the items which have same field dependence. Then Eq. (30) can be expressed as Eq. (31), which contains the Fringe Zernike coefficients.

#244275 Received 23 Jul 2015; revised 2 Sep 2015; accepted 2 Sep 2015; published 17 Sep 2015

$$\begin{bmatrix} W_{331M}\left(\vec{H}\cdot\vec{H}\right)\vec{H}-2\left(\vec{H}\cdot\vec{A}_{331M}\right)\vec{H}+\left(W_{131}+2B_{331M}\right)\vec{H} \\ -\left(\vec{H}\cdot\vec{H}\right)\vec{A}_{331M}+\vec{B}^{2}_{331M}\vec{H}^{*}-\left(\vec{A}_{131}+\vec{C}_{331M}\right) \end{bmatrix}=\begin{bmatrix} 3C_{coma,\mathrm{x}} \\ 3C_{coma,\mathrm{y}} \end{bmatrix}. \tag{31}$$

Equation (31) can be rewritten in a more compact matrix form:

$$\mathbf{H}_{COMA}\mathbf{P}_{COMA}=\mathbf{Z}_{COMA}, \tag{32}$$

where

$$\mathbf{H}_{COMA}=\begin{bmatrix} -3\vec{H}_x^{\,2}-\vec{H}_y^{\,2} & -2\vec{H}_x\vec{H}_y \\ -2\vec{H}_x\vec{H}_y & -\vec{H}_x^{\,2}-3\vec{H}_y^{\,2} \\ -1 & 0 \\ 0 & -1 \\ \vec{H}_x & -\vec{H}_y \\ \vec{H}_y & \vec{H}_x \\ \vec{H}_x^{\,3}+\vec{H}_x\vec{H}_y^{\,2} & \vec{H}_x^{\,2}\vec{H}_y+\vec{H}_y^{\,3} \\ \vec{H}_x & \vec{H}_y \end{bmatrix}^T, \mathbf{P}_{COMA}=\begin{bmatrix} \vec{A}_{331M,x} \\ \vec{A}_{331M,y} \\ \vec{A}_{131,x}+\vec{C}_{331M,x} \\ \vec{A}_{131,y}+\vec{C}_{331M,y} \\ \vec{B}^{2}_{331M,x} \\ \vec{B}^{2}_{331M,y} \\ W_{331M} \\ W_{131}+2B_{331M} \end{bmatrix} \text{ and } \mathbf{Z}_{COMA}=\begin{bmatrix} 3C_{coma,\mathrm{x}} \\ 3C_{coma,\mathrm{y}} \end{bmatrix}.$$

As one can see, $\mathbf{P}_{COMA}$ is a matrix with 8 rows and 1 column. So in order to fully characterize the 5th order coma aberration field, there are 7 unknowns need to be solve except W_{331M}. Wavefront measurements at a minimum of 4 field points are required.

5.2 Astigmatism

In the 5th order wave aberration expansions, the item which has the same aperture dependence as 3rd order astigmatism is quartic astigmatism (W_{422}). Its wave aberration expansion is

$$W_{AST5}=\begin{bmatrix} \frac{1}{2}W_{422}\left(\vec{H}\cdot\vec{H}\right)\vec{H}^{2}-\left(\vec{H}\cdot\vec{H}\right)\left(\vec{H}\vec{A}_{422}\right)+\frac{3}{2}\left(\vec{H}\cdot\vec{H}\right)\vec{B}^{2}_{422}-\left(\vec{H}\cdot\vec{A}_{422}\right)\vec{H}^{2} \\ -\frac{1}{2}\vec{C}^{3}_{422}\vec{H}^{*}+\frac{3}{2}B_{422}\vec{H}^{2}-\frac{3}{2}\left(\vec{H}\vec{C}_{422}\right)+\frac{1}{2}\vec{D}^{2}_{422} \end{bmatrix}\cdot\vec{\rho}^{2}, \tag{33}$$

where $W_{422}=\sum_j W_{422j}$, $\vec{A}_{422}=\sum_j W_{422j}\vec{\sigma}_j$, $\vec{B}^{2}_{422}=\sum_j W_{422j}\vec{\sigma}_j^{\,2}$, $\vec{C}^{3}_{422}=\sum_j W_{422j}\vec{\sigma}_j^{\,3}$, $B_{422}=\sum_j W_{422j}\left(\vec{\sigma}_j\cdot\vec{\sigma}_j\right)$, $\vec{C}_{422}=\sum_j W_{422j}\left(\vec{\sigma}_j\cdot\vec{\sigma}_j\right)\vec{\sigma}_j$, $\vec{D}^{2}_{422}=\sum_j W_{422j}\left(\vec{\sigma}_j\cdot\vec{\sigma}_j\right)\vec{\sigma}_j^{\,2}$.

We can sum the 3rd order astigmatism and the quartic astigmatism together, and merge the items which have same field dependence. Then Eq. (33) can be expressed as Eq. (34), which contains the Fringe Zernike coefficients,

$$\begin{bmatrix} \frac{1}{2}W_{422}\left(\vec{H}\cdot\vec{H}\right)\vec{H}^{2}-\left(\vec{H}\cdot\vec{H}\right)\left(\vec{H}\vec{A}_{422}\right)+\frac{3}{2}\left(\vec{H}\cdot\vec{H}\right)\vec{B}^{2}_{422}-\left(\vec{H}\cdot\vec{A}_{422}\right)\vec{H}^{2}-\frac{1}{2}\vec{C}^{3}_{422}\vec{H}^{*} \\ +\left(\frac{1}{2}W_{222}+\frac{3}{2}B_{422}\right)\vec{H}^{2}-\left(\vec{A}_{222}+\frac{3}{2}\vec{C}_{422}\right)\vec{H}+\left(\frac{1}{2}\vec{D}^{2}_{422}+\frac{1}{2}\vec{B}^{2}_{222}\right) \end{bmatrix}=\begin{bmatrix} C_{AST,x} \\ C_{AST,\mathrm{y}} \end{bmatrix}. \tag{34}$$

Equation (34) can be rewritten in a more compact matrix form:

$$\mathbf{H}_{AST}\mathbf{P}_{AST}=\mathbf{Z}_{AST}, \tag{35}$$

where

#244275 Received 23 Jul 2015; revised 2 Sep 2015; accepted 2 Sep 2015; published 17 Sep 2015

$$\mathbf{H}_{AST}=\begin{bmatrix} \vec{H}_x^{\,4}-\vec{H}_y^{\,4} & 2\vec{H}_x\vec{H}_y\left(\vec{H}_x^{\,2}+\vec{H}_y^{\,2}\right) \\ 3\vec{H}_x^{\,2}+3\vec{H}_y^{\,2} & 0 \\ 0 & 3\vec{H}_x^{\,2}+3\vec{H}_y^{\,2} \\ -\vec{H}_x & \vec{H}_y \\ -\vec{H}_y & -\vec{H}_x \\ \vec{H}_x^{\,2}-\vec{H}_y^{\,2} & 2\vec{H}_x\vec{H}_y \\ -\vec{H}_x & -\vec{H}_y \\ \vec{H}_y & -\vec{H}_x \\ 1 & 0 \\ 0 & 1 \\ -4\vec{H}_x^{\,3} & -6\vec{H}_x^{\,2}\vec{H}_y-2\vec{H}_y^{\,3} \\ 4\vec{H}_y^{\,3} & -2\vec{H}_x^{\,3}-6\vec{H}_x\vec{H}_y^{\,2} \end{bmatrix}^T,\mathbf{P}_{AST}=\begin{bmatrix} W_{422} \\ \vec{B}_{422,x}^2 \\ \vec{B}_{422,y}^2 \\ \vec{C}_{422,x}^3 \\ \vec{C}_{422,y}^3 \\ W_{222}+3B_{422} \\ 2\vec{A}_{222,x}+3\vec{C}_{422,x} \\ 2\vec{A}_{222,y}+3\vec{C}_{422,y} \\ \vec{D}_{422,x}^2+\vec{B}_{222,x}^2 \\ \vec{D}_{422,y}^2+\vec{B}_{222,y}^2 \\ \vec{A}_{422,x} \\ \vec{A}_{422,y} \end{bmatrix},\mathbf{Z}_{AST}=\begin{bmatrix} 2C_{AST,x} \\ 2C_{AST,y} \end{bmatrix}.$$

As one can see, $\mathbf{P}_{AST}$ is a matrix with 12 rows and 1 column. So in order to fully characterize the 5th aberration field, there are 11 unknowns need to be solved except W_{422}. Wavefront measurements at a minimum of 6 field points are required.

Utilizing Eqs. (17)-(23), (32) and (35), if the wavefronts are measured at multiple field points, an overdetermined system of nonlinear equations with 8 unknown misalignments can be established. As it is done in the 3rd order model, the medium-scale fminunc algorithm in the MATLAB Optimization Toolbox is used to solve the system of nonlinear equations.

5.3 Calculation of aberration coefficients

Before solving the misalignments by 5th order NAT model, we should know the 3rd and 5th order aberration coefficients of each surface in the system: W_{131}, W_{331M}, W_{222} and W_{422}. The 3rd order aberration coefficients can be calculated with Seidel formulas, but the 5th aberration coefficients are more difficult to calculate than the 3rd order coefficients. They consist of intrinsic surface contributions and induced contributions. The intrinsic aberrations depend only on properties of an optical surface. The induced aberrations depend on the sum of combinations of 3rd order image and pupil aberrations preceding the surface of interest. José Sasián [18] discussed the calculation of 5th order aberration (6th order wave aberration) coefficients, but we don't intend to use this method, either because the calculated process is complex, there may be calculation error, or because small higher than 3rd and 5th order aberrations exist in the system. Although the higher order aberrations are very small, their existence can still affect the accuracy of the calculation model.

For the reasons above, another method will be used in this paper. We are going to simulate a mass of random misaligned systems by using optical design software Code V. The aberration coefficients can be calculated based on the wavefronts of the misaligned system. The advantage of this method is that the model can describe the mathematic relation between misalignments and Zernike coefficients more realistically and accurately.

$\mathbf{P}_{COMA}/\mathbf{P}_{AST}$ can be further expressed as the product of two matrixes:

$$\mathbf{P}_{COMA}=\mathbf{S}_{COMA}\mathbf{W}_{COMA}, \tag{36}$$

$$\mathbf{P}_{AST}=\mathbf{S}_{AST}\mathbf{W}_{AST}. \tag{37}$$

$\mathbf{S}_{COMA}/\mathbf{S}_{AST}$ contains only the aberration field decenter vectors, and $\mathbf{W}_{COMA}/\mathbf{W}_{AST}$ is composed of the aberration coefficients.

If the number of the misaligned systems is n, and the number of field points for testing is m, Eqs. (38) and (39) can be obtained,

#244275 Received 23 Jul 2015; revised 2 Sep 2015; accepted 2 Sep 2015; published 17 Sep 2015

$$\begin{pmatrix} \begin{pmatrix} {}_1\mathbf{H}_{COMA} \\ \vdots \\ {}_m\mathbf{H}_{COMA} \end{pmatrix} & & \\ & \ddots & \\ & & \begin{pmatrix} {}_1\mathbf{H}_{COMA} \\ \vdots \\ {}_m\mathbf{H}_{COMA} \end{pmatrix} \end{pmatrix}_{2mn\times 8n} \begin{pmatrix} \mathbf{S}_{COMA}{}^{(1)} \\ \vdots \\ \mathbf{S}_{COMA}{}^{(n)} \end{pmatrix}_{8n\times 12} (\mathbf{W}_{COMA})_{12\times 1} = \begin{pmatrix} \begin{pmatrix} {}_1\mathbf{Z}_{COMA}{}^{(1)} \\ \vdots \\ {}_m\mathbf{Z}_{COMA}{}^{(1)} \end{pmatrix} \\ \vdots \\ \begin{pmatrix} {}_1\mathbf{Z}_{COMA}{}^{(n)} \\ \vdots \\ {}_m\mathbf{Z}_{COMA}{}^{(n)} \end{pmatrix} \end{pmatrix}_{2mn\times 1}, \tag{38}$$

$$\begin{pmatrix} \begin{pmatrix} {}_1\mathbf{H}_{AST} \\ \vdots \\ {}_m\mathbf{H}_{AST} \end{pmatrix} & & \\ & \ddots & \\ & & \begin{pmatrix} {}_1\mathbf{H}_{AST} \\ \vdots \\ {}_m\mathbf{H}_{AST} \end{pmatrix} \end{pmatrix}_{2mn\times 12n} \begin{pmatrix} \mathbf{S}_{AST}{}^{(1)} \\ \vdots \\ \mathbf{S}_{AST}{}^{(n)} \end{pmatrix}_{12n\times 12} (\mathbf{W}_{AST})_{12\times 1} = \begin{pmatrix} \begin{pmatrix} {}_1\mathbf{Z}_{AST}{}^{(1)} \\ \vdots \\ {}_m\mathbf{Z}_{AST}{}^{(1)} \end{pmatrix} \\ \vdots \\ \begin{pmatrix} {}_1\mathbf{Z}_{AST}{}^{(n)} \\ \vdots \\ {}_m\mathbf{Z}_{AST}{}^{(n)} \end{pmatrix} \end{pmatrix}_{2mn\times 1}, \tag{39}$$

where the bottom-left subscripts denote the different field points, while the top-right subscripts denote the different misaligned states. Equations (38) and (39) can be rewritten in more compact matrix forms as

$$\mathbf{H}'_{COMA}\mathbf{S}'_{COMA}\mathbf{W}_{COMA} = \mathbf{Z}'_{COMA}, \tag{40}$$

$$\mathbf{H}'_{AST}\mathbf{S}'_{AST}\mathbf{W}_{AST} = \mathbf{Z}'_{AST}. \tag{41}$$

The coma aberration coefficients $W_{131,j}$ and $W_{331M,j}$ and the astigmatism aberration coefficients $W_{222,j}$ and $W_{422,j}$ can be calculated by Eqs. (42) and (43),

$$\mathbf{W}_{COMA} = pinv(\mathbf{H}'_{COMA}\mathbf{S}'_{COMA})\mathbf{Z}'_{COMA}, \tag{42}$$

$$\mathbf{W}_{AST} = pinv(\mathbf{H}'_{AST}\mathbf{S}'_{AST})\mathbf{Z}'_{AST}, \tag{43}$$

where *pinv* denotes the Moore-Penrose pseudoinverse.

We simulate 1000 misaligned systems, and the number of field points for testing are 9, Table 4. gives the calculated aberration coefficients.

Table 4. Calculated Aberration Coefficients

	$W^{sph}_{131,j}$	$W^{asph}_{131,j}$	$W^{sph}_{331M,j}$	$W^{asph}_{331M,j}$	$W^{sph}_{222,j}$	$W^{asph}_{222,j}$	$W^{sph}_{422,j}$	$W^{asph}_{422,j}$
PM	−424.944	−2.660	−2.198	1.444	6.088	0.263	0.064	−0.030
SM	184.273	206.066	10.991	−0.278	−8.939	11.754	−0.289	−0.038
TM	−36.157	73.575	22.635	−32.691	19.442	−28.565	−0.520	0.779
sum	0.152		−0.098		0.043		−0.033	

The aberration coefficients are computed at a field angle of 0.18°, at a wavelength of 1 μm, which are in waves.

As one can see, in the calculated 5th order aberration coefficients, the value of $W_{331M,j}$ is large. It further illustrates the reason of inaccuracy of the 3rd order alignment model is that it ignores the influence of 5th order aberration.

5.4 Alignment example

In this section, we also use the misaligned system as shown in Table 3 to compare the 5th order model with the 3rd order model, and the same 9 field points for testing are used as before. We make 5 alignments on the misaligned TMA telescope in a row as well. The results are shown in Figs. 7(a)-7(c).

#244275 Received 23 Jul 2015; revised 2 Sep 2015; accepted 2 Sep 2015; published 17 Sep 2015

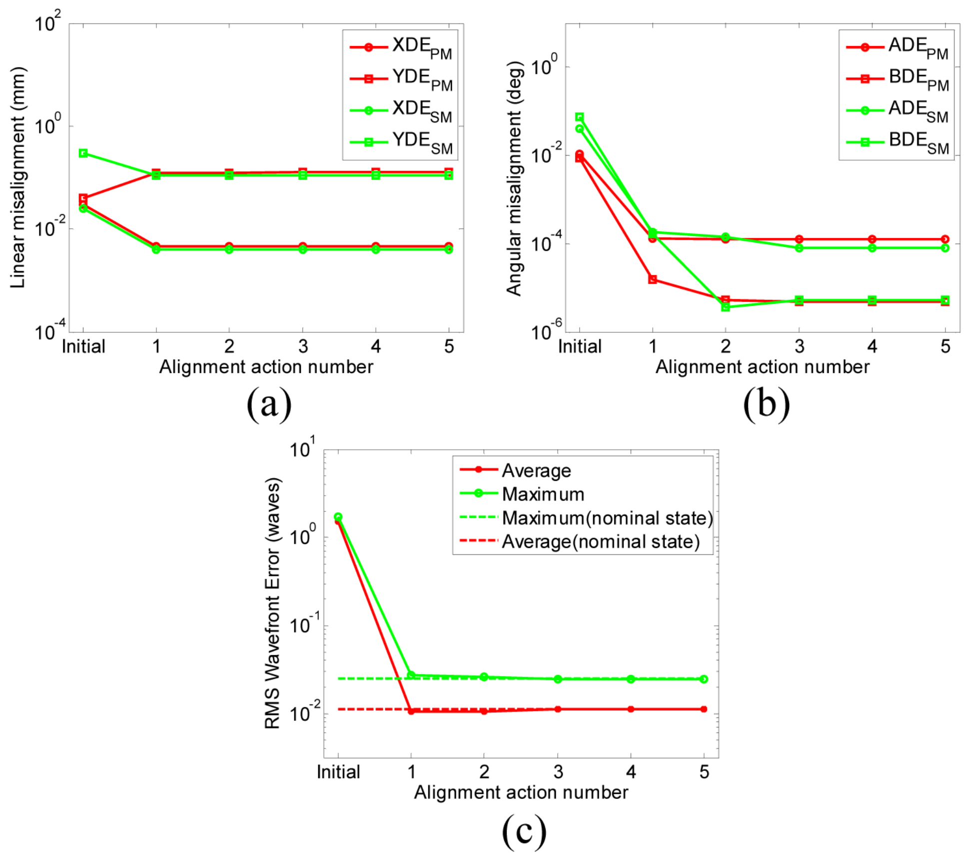

Fig. 7. The results after each alignment action. (a) The residual linear misalignments (b) The residual angular misalignments (c) The residual RMS wavefront error.

In order to facilitate comparison, the residual misalignments and the RMS wavefront errors after alignment corrections by the 3rd and the 5th order model are shown in Table 5.

Table 5. Alignment Results of the 3rd Order Model after the 4th Alignment Action and the 5th Order Model after the 3rd Alignment Action

	Nominal system	Original misaligned system	3rd order model	5th order model
XDE_{PM} (mm)	-	0.03	0.0019	–0.0046
YDE_{PM} (mm)	-	–0.04	0.1459	0.1259
ADE_{PM} (deg)	-	–0.011	–0.0002	0.0001
BDE_{PM}(deg)	-	0.009	–0.0001	0
XDE_{SM} (mm)	-	0.025	–0.0116	–0.0040
YDE_{SM} (mm)	-	0.3	0.0861	0.1098
ADE_{SM}(deg)	-	–0.04	–0.0041	0.0001
BDE_{SM}(deg)	-	0.075	0.0007	0
Average (waves)	0.011	1.504	0.063	0.011
Maximum (waves)	0.025	1.719	0.068	0.025

As a result, All the residual misalignments except YDE_{SM} after alignment corrections with the 5th order model are less than those with 3rd order model. The RMS wavefront error obviously decreases after only one alignment action. In the next 4 alignments, the change of the RMS wavefront error is not obvious. After the 3rd alignment action, the residual RMS wavefront error reaches the design level, and then the maximum and the average RMS wavefront error in the whole field of view are 0.025 λ and 0.011 λ, respectively. Overall, compared with the 3rd order model, the maximum and the average RMS wavefront error of the 5th order model are 37% and 17% of those of 3rd order model. All the residual angular misalignments after the 3rd alignment acton are very small, which are less than 0.0001°, but the individual residual linear misalignments are relatively large, such as YDE_{PM} and YDE_{SM}. The reason is that there is cross-coupling among the alignment parameters in the multiple mirrors system. Different types of misalignments can compensate each other.

In conclusion, although the elements of the TMA system are misaligned after alignments, the misalignments don't affect imaging performance. So this alignment is successful. Due to the influences of 5th order aberration is considered, the 5th order model has advantages over the 3rd order model, and its alignment capability for misaligned system is excellent.

6. Monte-Carlo alignment simulations

In engineering practice, the misalignments of optical elements are random variables, the size of which is closely related to the accuracy of coarse alignment. We discussed the performance of the two models in specific case in order to make a comparison before. The randomness of misalignments is ignored, and how the size of misalignments can affect the performance of the 5th order model is not discussed.

In order to analyze alignment performance of the 5th order model more comprehensively and objectively, Monte-Carlo alignment simulations are conducted in this section. The ranges of simulation misalignments are indicated in Table 6. There are 3 cases:

Table 6. Ranges of Misalignment Variables used for the Simulations

	Linear misalignment (mm)	Angular misalignment (deg)
Case 1	[-0.1,0.1]	[-0.01,0.01]
Case 2	[-0.5,0.5]	[-0.05,0.05]
Case 3	[-1,1]	[-0.1,0.1]

We generate 100 pairs of pseudorandom misalignment values following a standard uniform distribution for each case. Each of these misalignment states is introduced in the simulation software Code V and the resulting wavefronts can be obtained. As a result, we have 300 pairs of misalignments for all cases. The 300 misaligned systems are aligned by use of the 5th order NAT model, and we make 4 alignment actions on each misaligned TMA in a row. The alignment results are shown in Figs. 8(a)-8(c).

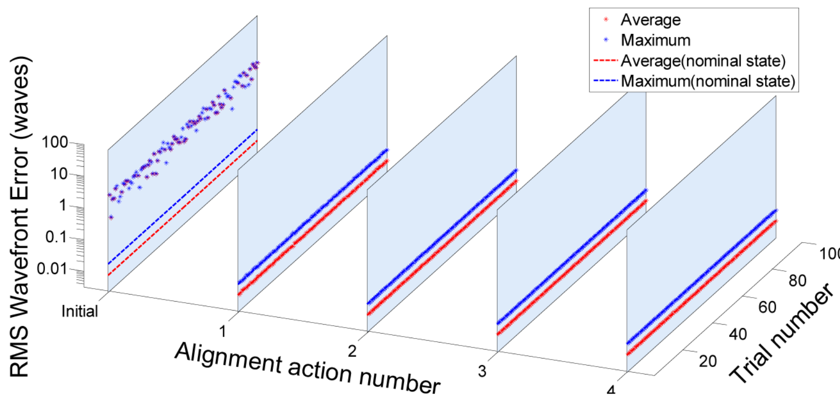

(a)

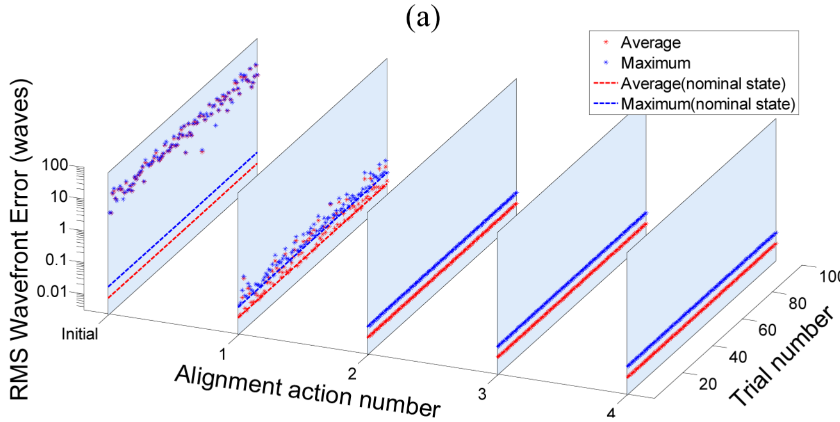

(b)

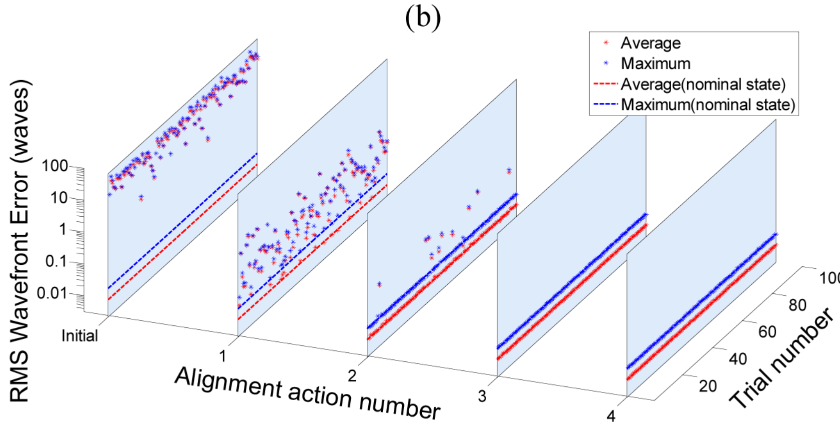

(c)

Fig. 8. The results of Monte-Carlo alignment simulations in the (a) case 1 (b) case 2 (c) case 3.

It can be seen from Figs. 8(a)-8(c) that the 5th order model has good performance in all 3 cases. The maximum and the average RMS wavefront error in the whole field of view can both reach design level. As seen in Fig. 8(a), in the case 1, due to the misalignment variables are small, RMS wavefront error of the TMA system can reach design level by only one alignment action.

As seen in Figs. 8(b) and 8(c), when the misalignment variables increase gradually, the difficulty in misalignments computation is obviously increased too. The system can't be well aligned by only one alignment action, and multiple iterative alignments are needed. In the

#244275 Received 23 Jul 2015; revised 2 Sep 2015; accepted 2 Sep 2015; published 17 Sep 2015

alignment process, each alignment action is accompanied by the decrease of RMS wavefront error. In our simulations, we need two alignment actions in case 2, while three alignment actions are needed in case 3.

In the alignment simulations, it is also found that serious vignetting will be introduced when misalignment variables continue to increase (e.g. ADE_{PM} = 0.2°). Serious vignetting can change the shape of the pupil, which causes inaccurate Zernike coefficients or even the Zernike coefficients cannot be calculated by Code V. So the maximum values of misalignments allowed are limited by vignetting.

7. Conclusion

In this paper, a novel alignment model for TMA systems is established based on 5th order NAT. The analytical expressions for aberration field decenter vectors and boresight error of misaligned TMA telescopes are derived. Two alignment models based on 3rd and 5th order NAT are established successively. The alignment process is shown in Fig. (9).

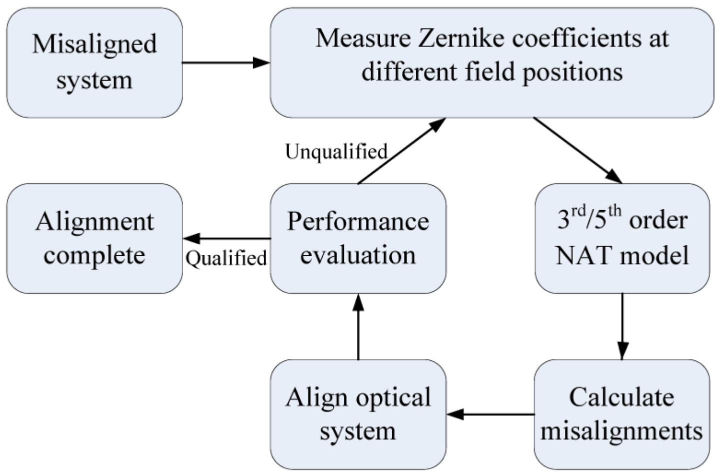

Fig. 9. The alignment process with 3rd/5th order NAT model.

It is found that one wavefront measurement is required to fully characterize the coma aberration field and two for the astigmatism aberration field as 3rd order model is used; and four for the coma aberration field and six for the astigmatism aberration field as 5th order model is used respectively. We compare the performance of 3rd order model with the 5th order model in an alignment example. The results show that the average and the maximum RMS wavefront errors in the whole field of view of 0.3° × 0.15° are 0.063 λ and 0.068 λ respectively after the 4th alignment action with 3rd order model, and 0.011 λ and 0.025 λ (nominal values) respectively after the 3rd alignment action with 5th order model. All the residual angular misalignments after the 3rd alignment action with 5th order model are less than 0.0001°. Individual residual linear misalignments are larger than 0.1 mm, because there is cross-coupling among the alignment parameters in the multiple mirrors system. The computational accuracy of misalignments of 5th order model is of better quality than that of the 3rd order model. It is because the 5th order aberration can't be ignored if we want to calculate misalignments accurately. For demonstration purposes Monte-Carlo alignment simulations are conducted. Simulation results show that the 5th order model still has good performance when the values of the misalignments are large (−1 mm ≤linear misalignment≤1 mm, −0.1°≤angular misalignment≤0.1°), and multiple iterative alignments are needed when the misalignment variables increase. In conclusion, not only can the NAT describe the aberration field characteristics of misaligned system, but also it can calculate misalignments quantitatively. The 5th order model can provide a reference basis for alignment of the TMA telescopes.

#244275 Received 23 Jul 2015; revised 2 Sep 2015; accepted 2 Sep 2015; published 17 Sep 2015

8. Appendix

Table 7

Table 7. Acronyms and Parameter Definitions

Acronyms		
FFDs	Full-Field-Displays: this type of display plots the magnitude and orientation of specific components of a Zernike coefficient decomposition of the wavefront created by tracing a grid of real rays over a grid of field points.	
NAT	Nodal Aberration Theory	
OAR	optical axis ray: initiates from the center of the object and passes through the center of the aperture stop.	
PM	primary mirror	
SM	secondary mirror	
TM	tertiary mirror	
TMA	three-mirror anastigmatic	
Paraxial/Constructional Quantities		
r_j	radius of surface j	
c_j	curvature of surface j $(1/r_j)$	
d_j	thickness of surface j	
$\bar{u}_j$	paraxial chief ray angle incident at surface j	
$\bar{y}_j$	chief ray height at surface j	
$\bar{i}_j$	paraxial incident angle of the chief ray at surface j	
Parameters of Perturbed (Misaligned) System		
$\overrightarrow{\beta_{0\ j}^{\#}}$	equivalent tilt of surface j	
$\overrightarrow{\delta v_j}^{*}$	intersection height of the OAR with respect to the aspheric vertex of surface j	
$\vec{\sigma}_j$	aberration field decenter vector of surface j	
$\Delta\vec{H}_{IMG}$	boresight error (image plane displacement)	
$\overrightarrow{\bar{i}_j^{*}}$	incident angle of the OAR at surface j	
OAR Quantities		
$\overrightarrow{\bar{u}_{OAR\ j}^{\#}}$	OAR paraxial angle prior to surface j referenced to the z-axis	
$\overrightarrow{\bar{y}_{OAR\ j}^{\#}}$	OAR intersection height at surface j referenced to the z-axis	
Perturbation Vectors and Scalars in NAT		
$\vec{A}_{klm} = \sum_j W_{klm_j} \vec{\sigma}_j$	$B_{klm} = \sum_j W_{klm_j} \left(\vec{\sigma}_j \cdot \vec{\sigma}_j\right)$	$\vec{B}_{klm}^{2} = \sum_j W_{klm_j} \vec{\sigma}_j^{\,2}$
$\vec{C}_{klm} = \sum_j W_{klm_j} \left(\vec{\sigma}_j \cdot \vec{\sigma}_j\right) \vec{\sigma}_j$	$\vec{C}_{klm}^{3} = \sum_j W_{klm_j} \vec{\sigma}_j^{\,3}$	$\vec{D}_{klm}^{2} = \sum_j W_{klm_j} \left(\vec{\sigma}_j \cdot \vec{\sigma}_j\right) \vec{\sigma}_j^{\,2}$

Acknowledgment

This work was supported by the National High Technology Research & Development Program of China (Grant NO.2011AA12A103).

#244275 Received 23 Jul 2015; revised 2 Sep 2015; accepted 2 Sep 2015; published 17 Sep 2015